Proceedings of Science and Mathematics
Faculty of Science, Universiti Teknologi Malaysia
Vol. 23, 2024, page 39-50

Magnetic Field and Heat Generation Effects on Squeezing Casson Hybrid Nanofluid Flow between Two Parallel Plates

Saidatul Wafiqah Ruzaidi, Mohd Ariff Admon
Department of Mathematical Sciences, Faculty of Science, Universiti Teknologi Malaysia
Corresponding author: ariffadmon@utm.my

Abstract
In the field of fluid dynamics, heat transfer and nanotechnology, there is a growing need to study the behaviour between magnetic fields, heat generation, and nanofluid flow. A model involving two-dimensional, incompressible magnetohydrodynamic squeezing flow of Casson hybrid nanofluid between two parallel plates is considered in this study. The lower plate has the capacity to stretch, while the upper plate moves towards the lower plate with a linear velocity in this model. Similarity transformation is utilized to reduce the governing dimensional partial differential equations into non-dimensional ordinary differential equations, then solved numerically through the bvp4c algorithm in MATLAB software. The effects of various physical parameters on the velocity profile, temperature distribution, skin friction coefficient and Nusselt number are examined. The validity of the results is then tested by comparing the numerical results of skin friction coefficients with previously published data, which resulting in a good agreement. The findings revealed that an increase in squeezing parameter Sq, suction/injection parameter S, stretching/shrinking parameter λ, and heat source/sink parameter Q, raises the temperature profile, while increasing the values of magnetic parameter M and Casson parameter β leads to a decrease in the temperature profile. For increasing value of λ, wall shear stress and heat transfer increases at the lower plate but decreases at the upper plate. Next, as M and Q increases, the wall shear stress declines at both plates while the heat transfer increases at lower plate and decrease at upper plate. Moreover, β are positively correlated with the wall shear stress at both plates, while for the heat transfer rate, it drops at the lower plate and rises at the upper plate. As for when M increases, the fluid velocity experiences deceleration at the lower plate, while exhibiting acceleration near the upper plate. The enhancement of M and S can lead to the development of the lower plate's heat transfer performance. Furthermore, when the concentrations of nanoparticles increase, the wall shear stress decreasing while heat transfer rate increasing. This behavior of the velocity and temperature profiles with various values of parameters are similar for both Casson parameters 0.5 (Casson hybrid nanofluid) and ∞ (hybrid nanofluid).
Keywords: Casson hybrid nanofluid; Magnetohydrodynamics; Squeezing flow; Parallel plates; Heat generation/absorption

Introduction

Heat transfer is the process of energy exchange between a system due to a difference in temperature and occured by conduction, convection or radiation [1]. Water is a typical example of a conventional fluid used in heat transfer applications, but it is less efficient compared to nanofluids that have enhanced thermal conductivity as well as thermal conductance coefficients [2][3]. The suspension of nanoparticles in fluids, generally called as nanofluids, has gain importance for increasing thermal conductivity particularly in usage of magnetic fields and heat production, thus creating the foundation of hybrid nanofluids [4]. Casson hybrid nanofluids as non-Newtonian fluids demonstrate potential in many applications due to their rheological characteristics[5][6]. Magnetohydrodynamics (MHD) also affects the fluids properties by imposing variations in flow field and heat transfer coefficients through the action of magnetic field.

In this research, the effects of magnetic fields, heat generation, and Casson hybrid nanofluids on squeezing flow, which is thoughtful for enhancing cooling methodologies in engineering context are discussed. There are several research articles published about the behavior of nanofluids and hybrid nanofluids in confined geometries that include squeezing flows. Because of their improved thermal capacity, these fluids are used in micro channels and heat exchangers among other uses [7][8][9]. The MHD squeezing flow, further modified by the impact of magnetic fields, offers novel avenues for improving heat transfer in hybrid nanofluids. In more detail, the compression flow of Casson hybrid nanofluids, which can be identified as highly effective and non-Newtonian, can be widely used for precise regulation of the characteristics of the fluids and their ability to transfer heat [10][11][12][13]. This paper intends to fill the research gaps in the analysis of the MHD squeezing flow of hybrid nanofluids with heat generation.

Numerous research studies also have been conducted on the flow behavior of Casson hybrid nanofluids under various conditions. The majority of research in fluid flow problem has focused on the squeezing flow of nanofluid and hybrid nanofluid. However, not all researchers have incorporated the influence of a magnetic field and heat generation into their investigations. Limited attention has been given to the study of the squeezing flow of Casson hybrid nanofluid, and, notably, the past discourse has yet to discuss the effect of both MHD and heat generation on squeezing flow of Casson hybrid nanofluid. Therefore, the primary objective of this study is to examine the effect of magnetic field and heat generation on squeezing flow of Casson hybrid nanofluid between two parallel plates.

Firstly, the mathematical model for this problem is developed using governing equations. This involved utilizing copper and aluminum oxide nanoparticles in water where the impacts of magnetic fields and heat generation were investigated on the flow of fluids. Then, similarity transformation is utilized to reduce the governing dimensional partial differential equations (PDEs) into non-dimensional ordinary differential equations (ODEs), then solved numerically through the bvp4c algorithm in MATLAB software. The effects of various physical parameters such as Casson parameter β, squeezing number Sq, suction/injection parameter S, stretching/shrinking parameter λ, magnetic parameter M and heat source/sink parameter Q on the velocity profile, temperature profile, skin friction coefficient and Nusselt number are examined. The validity of the results is then tested by comparing the numerical results of skin friction coefficients with previously published data, which resulting in a good agreement.

The findings revealed that an increase in Sq, S, λ, and Q raises the temperature profile, while increasing the values of M and β leads to a decrease in the temperature profile. Next, as M and Q increases, the wall shear stress declines at both plates while the heat transfer increases at lower plate and decrease at upper plate. As for when M increases, the fluid velocity experiences deceleration at the lower plate, while exhibiting acceleration near the upper plate. Furthermore, when the concentrations of nanoparticles increase, the wall shear stress decreasing while heat transfer rate increasing.

This study contributes to the select area of fluid dynamics focusing on the impacts of magnetic fields, heat generation, and Casson hybrid nanofluids in squeezing flows. These results can be directly applied to enhance the heat transfer in engineering applications such as heat exchangers, and cooling systems [14]. This study has the potential to drive innovation and technological development in various industries, offering more efficient and sustainable solutions. Ultimately, the significance of this research extends to environmental considerations, as improvements in heat transfer efficiency can contribute to energy conservation and reduced environmental impact [15].

Mathematical Formulation

Governing Equations

Consider a dynamic scenario involving a two-dimensional, incompressible magnetohydrodynamic (MHD) squeezing flow of Casson hybrid nanofluid $(\mathrm{Cu}-\mathrm{Al_2O_3}/\mathrm{NaC_6H_7O_6})$ between two parallel plates. The lower plate is situated at $y=0$, while the upper plate is positioned at $y=h(t)=\sqrt{\frac{v_f(1-\alpha t)}{b}}$

from the lower plate. The lower plate has the capacity to stretch, and simultaneously, the upper plate moves towards the lower plate with a velocity of $V_h = \frac{dh(t)}{dt} = -\frac{\alpha}{2}\sqrt{\frac{v_f}{b(1-\alpha t)}}$. When $\alpha > 0$, both upper and lower plates are squeezed while separated when $\alpha < 0$ until $t = \frac{1}{a}$. Next, the temperatures of the lower and upper plates are maintained at fixed temperatures T_1 and T_2, respectively. Additionally, the possible fluid suction/injection of the lower plate, with the wall mass velocity, $v_w = -\frac{V_0}{1-\alpha t}$ is also considered, where $V_0 > 0$ indicates suction, $V_0 < 0$ denotes injection, and $V_0 = 0$ signifies an impermeable plate. For the lower plate, it is stretchable with linear velocity $u_w = \frac{bx}{1-\alpha t}$ when $t < \frac{1}{a}$ and the uniform magnetic field strength considered is $B(t) = \frac{B_0}{\sqrt{1-\alpha t}}$ where it is applied perpendicularly to the lower plate with constant B_0. The physical model and coordinate system are as shown in Figure 1.

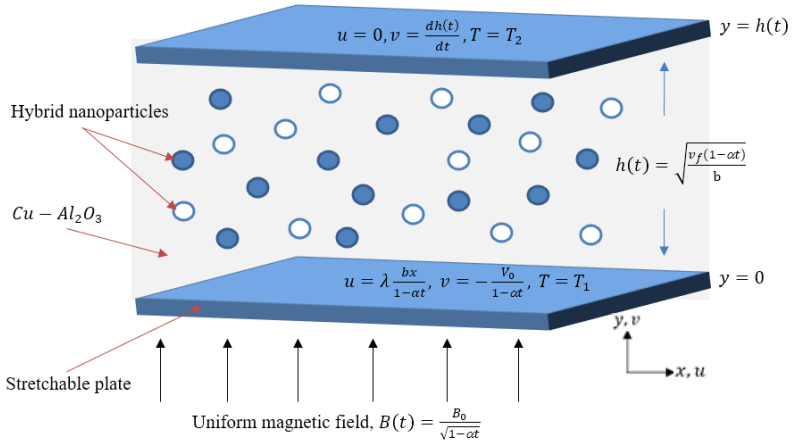

Figure 1 Physical model and coordinate system.

Under these assumptions and employing the hybrid nanofluid model proposed by [16][17][18], the governing conservation equations are as follows:

$$\frac{\partial u}{\partial x} + \frac{\partial v}{\partial y} = 0, \tag{1}$$

$$\frac{\partial V}{\partial t} + u\frac{\partial V}{\partial x} + v\frac{\partial V}{\partial y} = \frac{\mu_{hnf}}{\rho_{hnf}}\left(1 + \frac{1}{\beta}\right)\left(\frac{\partial^2 V}{\partial x^2} + \frac{\partial^2 V}{\partial y^2}\right) - \frac{\sigma_{hnf}}{\rho_{hnf}}B(t)^2 V, \tag{2}$$

$$\frac{\partial T}{\partial t} + u\frac{\partial T}{\partial x} + v\frac{\partial T}{\partial y} = \frac{k_{hnf}}{(\rho c_p)_{hnf}}\left(\frac{\partial^2 T}{\partial x^2} + \frac{\partial^2 T}{\partial y^2}\right) + \frac{Q^*}{(\rho c_p)_{hnf}}(T - T_0), \tag{3}$$

where, $V = \frac{\partial v}{\partial x} - \frac{\partial u}{\partial y}$. The associate boundary conditions used at the lower and upper plates are [16]:

$$\begin{aligned} u = \lambda\frac{bx}{1-\alpha t},\ v = -\frac{V_0}{1-\alpha t},\ T = T_1 \text{ at } y = 0, \\ u = 0,\ v = \frac{dh(t)}{dt},\ T = T_2 \text{ at } y = h(t), \end{aligned} \tag{4}$$

respectively.

Here, u and v represent the velocities along the x and y directions, respectively, and T denotes the temperature of the hybrid nanofluid. Specifically, μ_{hnf} denotes the dynamic viscosity of the hybrid nanofluid, while ρ_{hnf} represents its density. The Casson parameter is denoted by β, and σ_{hnf} signifies the electrical conductivity of the hybrid nanofluid. The magnetic field strength is expressed as $B(t)$. k_{hnf} represents the thermal conductivity of the hybrid nanofluid and the heat capacity of the hybrid

nanofluid is expressed as $(\rho c_p)_{hnf}$. Furthermore, the reference temperature for hybrid nanofluid flow is represented by T_0, and Q represents the coefficient of heat source/sink.

This study involves suspending nanoparticles of copper and aluminium oxide into Casson hybrid nanofluid $(\mathrm{Cu}-\mathrm{Al_2O_3}/\mathrm{NaC_6H_7O_6})$. The correlations for various properties of the hybrid nanofluid, including dynamic viscosity, density, heat capacity, electrical conductivity, and thermal conductivity are shown in Table 1. The correlations are referred from [19], which have been verified through experimental validation to ensure the feasibility and accuracy. In Table 2, the thermophysical properties of both the base fluid and nanoparticles adopted from studies by [20][21][22] are shown as below.

Table 1: Correlations of hybrid nanofluid.

Properties	Hybrid Nanofluid
Dynamic viscosity, μ	$\frac{\mu_{hnf}}{\mu_f} = (1-\phi_{hnf})^{-2.5}$
Density, ρ	$\rho_{hnf} = \left(1-\phi_{hnf}\right)\rho_f + \phi_1\rho_{s1} + \phi_2\rho_{s2}$
Heat capacity, ρC_p	$(\rho C_p)_{hnf} = \left(1-\phi_{hnf}\right)\left(\rho c_p\right)_f + \phi_1(\rho C_p)_{s1} + \phi_2(\rho C_p)_{s2}$
Electrical conductivity, σ	$\frac{\sigma_{hnf}}{\sigma_f} = \frac{\left(\frac{\phi_1\sigma_1+\phi_2\sigma_2}{\phi_{hnf}}\right)+2\sigma_f+2\left(\phi_1\sigma_1+\phi_2\sigma_2\right)-2\phi_{hnf}\sigma_f}{\left(\frac{\phi_1\sigma_1+\phi_2\sigma_2}{\phi_{hnf}}\right)+2\sigma_f-\left(\phi_1\sigma_1+\phi_2\sigma_2\right)+\phi_{hnf}\sigma_f}$
Thermal conductivity, k	$\frac{k_{hnf}}{k_f} = \frac{\left(\frac{\phi_1k_1+\phi_2k_2}{\phi_{hnf}}\right)+2k_f+2\left(\phi_1k_1+\phi_2k_2\right)-2\phi_{hnf}k_f}{\left(\frac{\phi_1k_1+\phi_2k_2}{\phi_{hnf}}\right)+2k_f-\left(\phi_1k_1+\phi_2k_2\right)+\phi_{hnf}k_f}$

Table 2: Thermophysical properties of base fluid and nanoparticles.

Thermophysical properties	Sodium alginate $\mathbf{NaC_6H_7O_6}$	Aluminium Oxide $\mathbf{Al_2O_3}$	Copper $\mathbf{Cu}$
ρ $(\mathrm{kgm^{-3}})$	989	3970	8933
C_p $(\mathrm{Jkg^{-1}K^{-1}})$	4175	765	385
σ $(\mathrm{sm^{-1}})$	2.6×10^{-4}	3.69×10^{7}	5.96×10^{7}
k $(\mathrm{Wm^{-1}K^{-1}})$	0.6376	40	400

Similarity Transformation

To transform the dimensional partial differential equations (PDEs) into nondimensional ordinary differential equations (ODEs), the utilization of the following dimensionless variables as described by [16] is employed,

$$\psi = \sqrt{\frac{bv_f}{1-\alpha t}}\, xf(\eta), u = \frac{bx}{1-\alpha t}f'(\eta), v = -\sqrt{\frac{bv_f}{1-\alpha t}}\, f(\eta), \eta = \sqrt{\frac{b}{v_f(1-\alpha t)}}\, y\,, \theta(\eta) = \frac{T-T_0}{T_2-T_0}, \tag{5}$$

where T_0 is the temperature for hybrid nanofluid flow. Next, substituting equation (5) into equations (2), (3) and (4), the ODEs and boundary conditions are:

$$\left(1+\frac{1}{\beta}\right)\left(\frac{\mu_{hnf}/\mu_f}{\rho_{hnf}/\rho_f}\right)f^{iv} + ff''' - f'f'' - \frac{Sq}{2}(\eta f''' + 3f'') - \left(\frac{\sigma_{hnf}/\sigma_f}{\rho_{hnf}/\rho_f}\right)Mf'' = 0, \tag{6}$$

$$\frac{1}{Pr}\left(\frac{k_{hnf}/k_f}{\left(\rho c_p\right)_{hnf}/\left(\rho c_p\right)_f}\right)\theta'' + f\theta' - \frac{Sq}{2}\eta\theta' + Q\left(\frac{1}{(\rho c_p)_{hnf}/(\rho c_p)_f}\right)\theta = 0, \tag{7}$$

$$f'(0) = \lambda, f(0) = S, \theta(0) = \delta, \tag{8a}$$

$$f'(1) = 0, f(1) = \frac{Sq}{2}, \theta(1) = 1, \tag{8b}$$

where, $\lambda > 0$ refers to stretching, $\lambda < 0$ indicates shrinking, and $\lambda = 0$ denotes a fixed/static position of the lower plate. Other dimensionless parameters include the squeezing parameter Sq, magnetic parameter M, Prandtl number Pr, heat source/sink parameter Q, suction/injection parameter S, and the temperature ratio parameter δ. These parameters are defined as follows:

$$Sq = \frac{\alpha}{b}, \quad M = \frac{\sigma_f {B_0}^2}{b\rho_f}, \quad Pr = \frac{v_f}{k_f/(\rho c_p)_f}, Q = \frac{Q^*}{(\rho c_p)_f}\frac{1-\alpha t}{b}, \quad S = \frac{V_0}{bh}, \quad \delta = \frac{T_1 - T_0}{T_2 - T_0}.$$

Physical Quantities

The physical quantities of interest under consideration are the skin friction coefficient and the Nusselt number, as defined by [17].

$$C_{fx} = \frac{\mu_{hnf}\left(1+\frac{1}{\beta}\right)\left(\frac{\partial u}{\partial y}\right)_{y=h(t)}}{\rho_f {V_h}^2}, \tag{9}$$

$$Nu_x = -\frac{k_{hnf} x \left(\frac{\partial T}{\partial y}\right)_{y=h(t)}}{k_f(T_2 - T_0)}. \tag{10}$$

Substituting equation (5) into equations (9) and (10), then the skin friction coefficient and Nusselt number at the lowest and upper plates are,

$$\text{Lower: } \frac{1}{4}\frac{\alpha^2}{b^2} C_{fx1} {Re_x}^{-\frac{1}{2}} = \frac{\mu_{hnf}}{\mu_f}\left(1+\frac{1}{\beta}\right) f''(0), \tag{11a}$$

$$\text{Upper: } \frac{1}{4}\frac{\alpha^2}{b^2} C_{fx2} {Re_x}^{-\frac{1}{2}} = \frac{\mu_{hnf}}{\mu_f}\left(1+\frac{1}{\beta}\right) f''(1), \tag{11b}$$

$$\text{Lower: } Nu_{x1} {Re_x}^{-\frac{1}{2}} = -\frac{k_{hnf}}{k_f}\theta'(0), \tag{12a}$$

$$\text{Upper: } Nu_{x2} {Re_x}^{-\frac{1}{2}} = -\frac{k_{hnf}}{k_f}\theta'(1). \tag{12b}$$

respectively, where $Re_x = \frac{x u_w}{v_f}$ is the local Reynolds number.

Numerical Computation and Validation

Equations (6), (7) and (8) are numerically solved by utilizing the bvp4c solver in MATLAB software. To solve this problem with bvp4c, we convert the ordinary differential equations, ODEs into a system of first-order ODEs by introducing new variables.

$$(y1, y2, y3, y4, y5, y6) = (f, f', f'', f''', \theta, \theta'). \tag{13}$$

Therefore, equations (6), (7) and (8) can be represented as,

$$f^{iv} = \left(\frac{\rho_{hnf}/\rho_f}{\mu_{hnf}/\mu_f}\right)\left(\frac{1}{1+\frac{1}{\beta}}\right)\left[\frac{Sq}{2}(\eta y4 + 3y3) + \left(\frac{\sigma_{hnf}/\sigma_f}{\rho_{hnf}/\rho_f}\right) M y3 - y1y4 + y2y3\right], \tag{14}$$

$$\theta'' = \Pr\left(\frac{(\rho c_p)_{hnf}/(\rho c_p)_f}{k_{hnf}/k_f}\right)\left[\frac{Sq}{2}\eta y6 - y1y6 - Q\left(\frac{1}{(\rho c_p)_{hnf}/(\rho c_p)_f}\right) y5\right], \tag{15}$$

subject to boundary conditions,

$$ya2 = \lambda, \quad ya1 = S, \quad ya5 = \delta, \tag{16a}$$

$$yb2 = 0, \quad yb1 = \frac{Sq}{2}, \quad yb5 = 1, \tag{16b}$$

where ya and yb represent the lower and upper plates boundary conditions respectively. An appropriate value for the step size is chosen such that $\Delta\eta$ = 0.01 and $\eta_\infty = 1$.

In order to verify the effectiveness of the bvp4c algorithm developed in MATLAB software, the numerical results of skin friction coefficient are cross-referenced with previously published results. Tables 3 and 4 shows the comparison of the skin friction coefficient at both lower and upper plates for various values

of M and S, aligning them with the findings of [23] and [16]. An excellent agreement between the results is shown through the comparison.

Table 3: Comparison of values of lower plate, $-(\mu_{hnf}/\mu_f)(1+\beta^{-1})f''(0)$ with $\mathrm{Pr}=6.2, Sq=\delta=0, \lambda=1,\ \phi_1\to 0,\ \phi_2\to -\infty,\ \beta\to\infty,\ Q=0$, with different values of M and S.

		$-\left(\frac{\mu_{hnf}}{\mu_f}\right)\left(1+\frac{1}{\beta}\right)f''(0)$		
M	S	**Present**	**[23]**	**[16]**
0	0.5	7.411153	7.411153	7.411153
1	0.5	7.591618	7.591618	7.591618
4	0	4.587891	4.587891	4.587891
4	0.3	6.665662	6.665662	6.665662
4	0.5	8.110334	8.110334	8.110334
4	0.6	8.851444	8.851444	8.851444
4	1	11.948584	11.948584	11.948584
9	0.5	8.910096	8.910096	8.910096

Table 4: Comparison of values of upper plate, $(\mu_{hnf}/\mu_f)(1+\beta^{-1})f''(1)$ with $\mathrm{Pr}=6.2, Sq=\delta=0,\ \lambda=1,\ \phi_1\to 0, \phi_2\to -\infty,\ \beta\to\infty,\ Q=0$, with different values of M and S.

		$\left(\frac{\mu_{hnf}}{\mu_f}\right)\left(1+\frac{1}{\beta}\right)f''(1)$		
M	S	**Present**	**[23]**	**[16]**
0	0.5	4.713303	4.713303	4.713303
1	0.5	4.739017	4.739017	4.739017
4	0	1.842447	1.842447	1.842447
4	0.3	3.653695	3.653695	3.653695
4	0.5	4.820251	4.820251	4.820251
4	0.6	5.391248	5.391248	5.391248
4	1	7.593426	7.593426	7.593426
9	0.5	4.964870	4.964870	4.964870

Results and Discussion

Velocity and Temperature Profiles

The effects of physical parameters such as Casson parameter β, squeezing number Sq, suction/injection parameter S, stretching/shrinking parameter λ, magnetic parameter M and heat source/sink parameter Q on the velocity profile $f'(\eta)$ and temperature profile $\theta(\eta)$ of the fluid flow are discussed. An analysis of the effects of each parameter in relation to others is conducted and the outcome patterns for the hybrid nanofluid with various parameter values is presented in Figures 2(a) to 7(b). Consequently, the parameters are set as follows: $\mathrm{Pr}=6.5,\ Sq=1, S=0.5\ \delta=0,\ \lambda=1, \phi_1=\phi_2=0.01, M=1,\ Q=0$. Meanwhile for β, two different cases are considered where β = 0.05 indicates Casson hybrid nanofluid while $\beta\to\infty$ indicates hybrid nanofluid.

Figure 2(a) illustrated the velocity profile $f'(\eta)$ of the fluid flow across various values corresponding to β. As β increases, the velocity presents a dual behavior at the lower and upper plates. Specifically, the velocity decreases at the lower plate η < 0.45, whereas it increases at the upper plate η > 0.45. This suggests that a higher value of β leads to an increased fluid viscosity, strengthening the resistance between the parallel plates and slowing down the fluid velocity. However, the changes in β near the upper plate do not affect the velocity since the adhesion of the fluid flow near upper plate is stronger compared to the cohesion. Therefore, the velocity near the upper plate increases due to the squeezing effect of the parallel plates. Figure 2(b) showed the influence of β on the temperature profile $\theta(\eta)$. As β increases, a decrease in the fluid temperature is observed at both the lower and upper plates. This

occurs because the higher viscosity strengthens the bonds between fluid particles, hence reducing their kinetic energy and resulting in a decline in the temperature profile.

In Figure 3(a), the impact of Sq is shown for three different values of β: 0.05, 1 and ∞ on the velocity profile. As Sq increases for all values of β, the velocity of the fluid also increases. When $Sq > 0$ and the plates move closer together, the fluid flows through the channel more rapidly, resulting in a higher velocity. Conversely, when $Sq < 0$ and the plates move apart, resistance in the wider channel increases, leading to a decrease in fluid velocity. Moreover, the figure also illustrates a significant rise in velocity for all Sq values when η is approximately between 0.4 to 0.5, and drops for other value of η due to the effect of β. A lower value of β corresponds to reduced viscosity, which in turn accelerates velocity near the lower plate. The impact of Sq on the temperature profile is illustrated in Figure 3(b). With increasing Sq, the fluid temperature decreases near the lower plate $\eta < 0.55$, while it increases near the upper plate $\eta > 0.55$, for three different values of β: 0.05, 1 and ∞. Initially, the velocity is high near the lower plate, resulting frequent collision between fluid particles, thus accumulating greater kinetic energy in the fluid particles. However, as the fluid velocity decreases when the plates move closer, physical changes occur in the fluid particles as the upper plate is squeezed toward the lower plate, leading to an increased in velocity. The limited distance between plates increases collision rate between fluid particles. Consequently, as the kinetic energy increases, the fluid temperature rises.

The impact of the parameter S on the velocity profile $f'(\eta)$ is shown in Figure 4(a). With the increase in S values, where $S < 0$ represents injection and $S > 0$ represent suction, the fluid velocity decreases for all three different values of β: 0.05, 1 and ∞. With the presence of Casson parameter β, fluid flow increases near the lower plate $\eta < 0.5$, while it decreases near the upper plate $\eta > 0.5$. The graph indicates that higher injection values enhance the velocity profile, making injection at the lower plate more effective in preventing boundary layer separation. Suction/injection is typically utilized to prevent boundary layer separation. In Figure 4(b), illustrations of the behavior of the temperature profile $\theta(\eta)$ across various values of the suction/injection parameter S are shown. From the graph, it can be seen that the fluid temperature increases with the increase in S for all three different values of β: 0.05, 1 and ∞, indicating a higher temperature for suction compared to injection. As suction removes layers separated from the boundary layer, fluid momentum is improved, leading to an increase in the temperature profile.

Figure 5(a) showed the velocity profiles for various values of the parameter λ. The shrinking of the lower plate is signified by $\lambda < 0$, while the stretching of lower plate is represented by $\lambda > 0$. As λ increases, a dual behavior in fluid velocity is observed. The velocity accelerates for $\eta < 0.3$ but decelerates after the transition point $\eta > 0.3$, for β values of 0.05, 1, and ∞. This indicates that the fluid velocity increases as the lower plate is stretched. Meanwhile, opposite behavior is observed near the upper plate. The behavior of temperature profile $\theta(\eta)$ with various values of λ is presented in Figure 5(b). With an increase in λ, the fluid temperature rises for all three different values of β: 0.05, 1 and ∞. This suggests that the temperature of fluid flow rises due to the lower plate being stretched.

Figure 6(a) illustrated the impact of various magnetic parameter M on the velocity profile $f'(\eta)$. With increasing values of M, the velocity decreases near the lower plate for all three different values of β: 0.05, 1 and ∞. As shown in the graph, when $\eta > 0.4$, the velocity increases with the rise in the magnetic parameter M. A significant decrease to the fluid flow could occur when a powerful magnetic field is applied to the lower plate. The magnetic field within the electrically conducting fluid generates Lorentz forces that oppose the fluid velocity, leading to its decrease. However, the velocity near the upper plate remains unaffected by the magnetic field, which is applied solely to the lower plate. Hence, the fluid velocity increases due to the squeezing effect. Figure 6(b) illustrated the effects of the magnetic parameter M on the temperature profile $\theta(\eta)$. It is observed that as the value of M increases, the fluid temperature decreases for all three different values of β: 0.05, 1 and ∞. The magnetic field that generate Lorentz forces, reduce the thermal diffusion. Similarly, when a strong magnetic field is applied to the lower plate, the fluid temperature declines.

Figure 7(a) analyzed the behavior of the velocity profile $f'(\eta)$ with various values of parameter Q. When $Q < 0$ which indicate a heat sink, the fluid flow faster near the wall and slower away from it due to cooling and densification of the fluid near the wall. Contrarily, when $Q > 0$ which indicate a heat source, the fluid

flow slower near the wall and faster away from it because of heating and expansion of the fluid near the wall. When Q = 0, the fluid flow is uniform. The figure also revealed that the higher the values of Q, the steeper the velocity gradient, signifying a quicker change in velocity with distance from the wall. Conversely, for lower values of Q, the gradient is less steep, indicating a more gradual change in velocity. Figure 7(b) shows the impact of Q on the temperature profile, $\theta(\eta)$. When Q < 0, the fluid experiences a cooling effect, resulting in lower temperatures compared to when Q = 0 where no heat source or sink. In contrast, positive values of when Q > 0 indicate a heating effect, leading to higher temperatures.

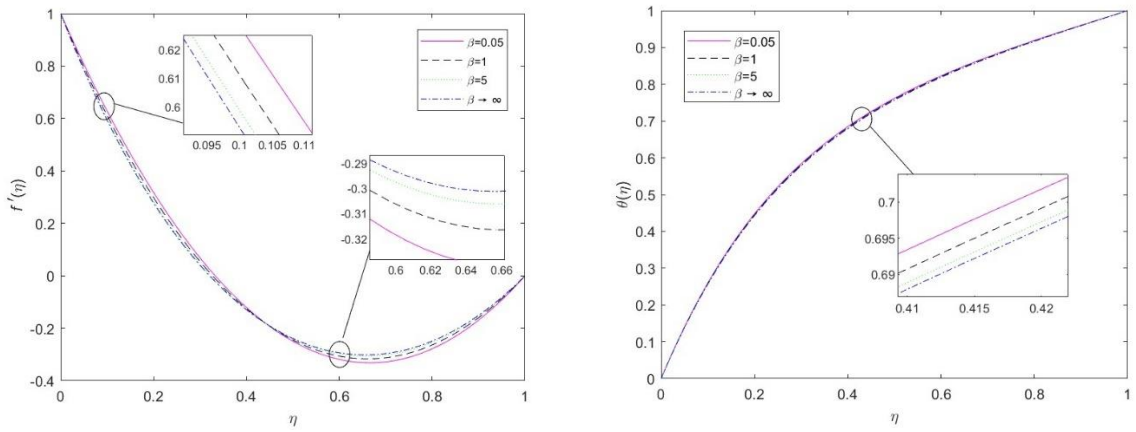

Figure 2 Impact of Casson parameter β on the (a) velocity $f'(\eta)$ and (b) temperature $\theta(\eta)$ profiles.

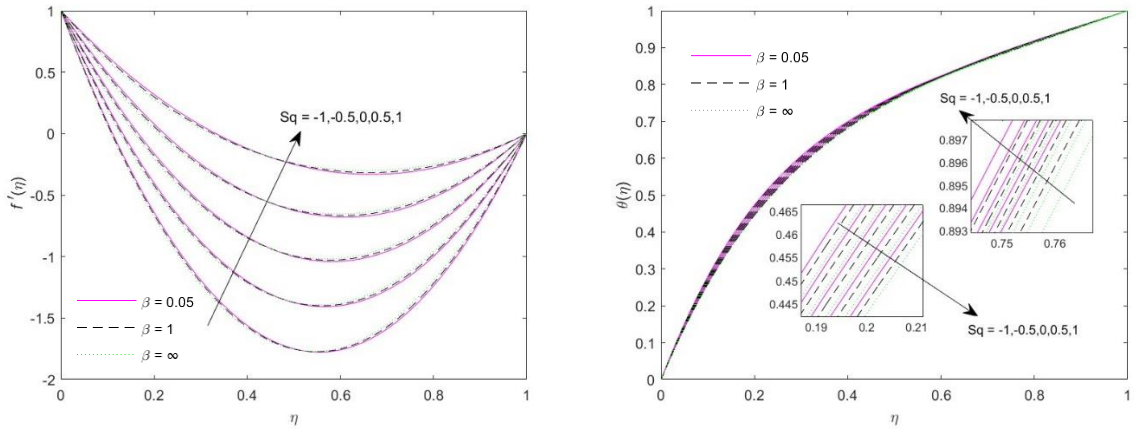

Figure 3 Impact of squeezing number Sq on the (a) velocity $f'(\eta)$ and (b) temperature $\theta(\eta)$ profiles.

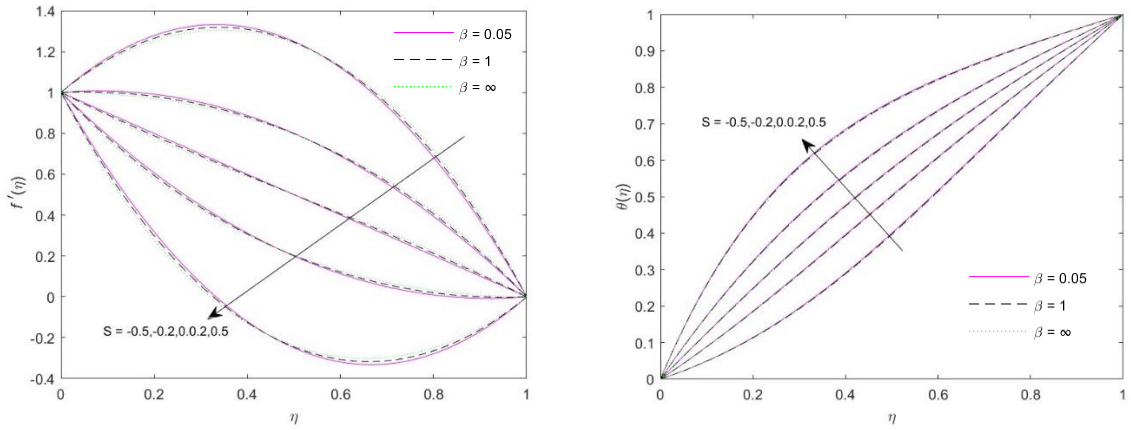

Figure 4 Impact of suction/injection parameter S on the (a) velocity $f'(\eta)$ and (b) temperature $\theta(\eta)$ profiles.

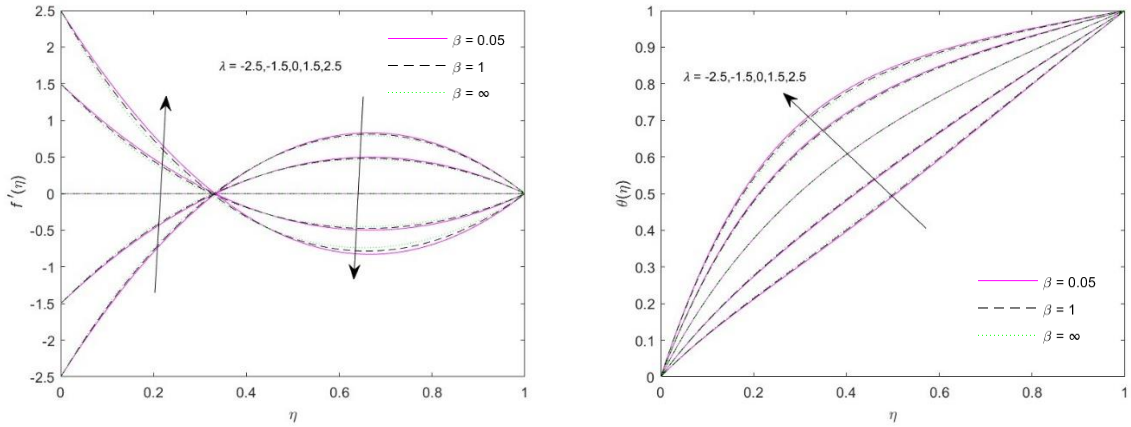

Figure 5 Impact of stretching/shrinking parameter λ on the (a) velocity $f'(\eta)$ and (b) temperature $\theta(\eta)$ profiles.

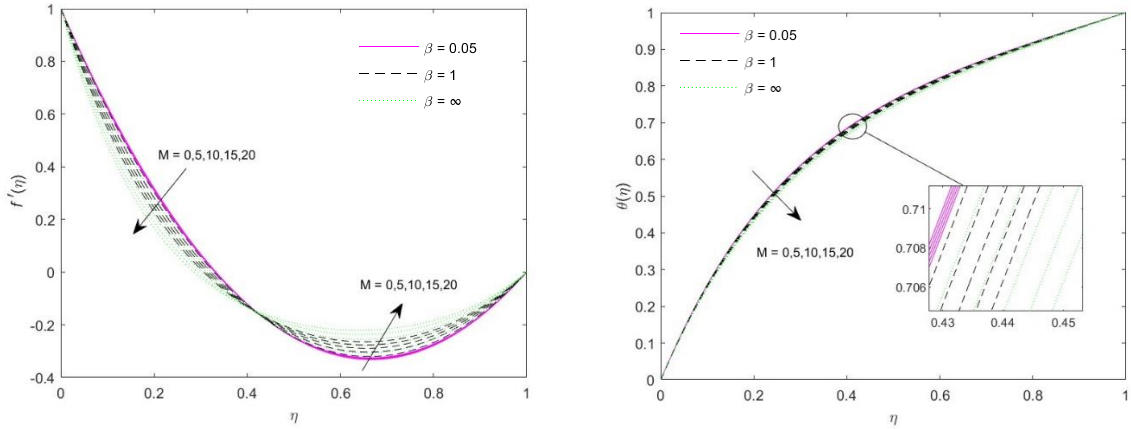

Figure 6 Impact of magnetic parameter M on the (a) velocity $f'(\eta)$ and (b) temperature $\theta(\eta)$ profiles.

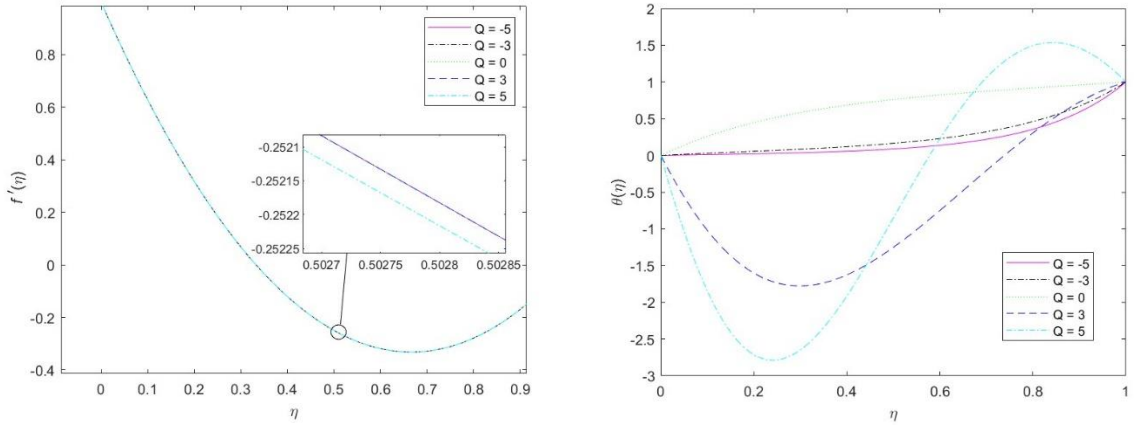

Figure 7 Impact of heat source/sink parameter Q on the (a) velocity $f'(\eta)$ and (b) temperature $\theta(\eta)$ profiles.

Skin Friction Coefficient and Nusselt Number

This study examines the effects of Sq, S, λ, M, β, Q, ϕ_1, ϕ_2 on the fluid flow. The skin friction coefficient indicates wall shear stress, and the Nusselt number represents the heat transfer rate. Numerical findings from the bvp4c solver in Matlab for various parameter values are presented in Table 4. For the numerical values of skin friction coefficients, as Sq increases, the wall shear stress rises at the lower plate and decreases at the upper plate. Next, an increase in S and a decrease in λ reduce the wall shear stress at the lower plate and increase it at the upper plate. M is negatively correlated with wall shear stress at both plates due to Lorentz forces. The increase in β raises wall shear stress at both plates, while Q has the opposite effect. Lastly, a higher concentration of Casson nanofluid ϕ_1 and ϕ_2 reduce the wall shear stress at both plates.

Table 4 also illustrated the numerical values of Nusselt number for various physical parameters and their effects on heat transfer rates at both plates. As Sq increases, heat transfer rates rise at both plates due to increased kinetic energy. Furthermore, an increase in S and λ increases the heat transfer at the lower plate and decreases it at the upper plate. As for when parameters M and Q increases, the heat transfer rise at the lower plate but decrease at the upper plate. Next, when β increases, the rate of heat transfer decreases at the lower plate and increases at the upper plate. A higher nanoparticle concentration, results in an increase in the heat transfer at both plates.

Table 4: Numerical values of skin friction coefficients and Nusselt number with various values of physical parameters.

Sq	S	λ	M	β	Q	ϕ_1	ϕ_2	$\frac{1}{4}\frac{\alpha^2}{b^2}C_{fx1}Re_x^{-\frac{1}{2}}$	$\frac{1}{4}\frac{\alpha^2}{b^2}C_{fx2}Re_x^{-\frac{1}{2}}$	$Nu_{x1}Re_x^{-\frac{1}{2}}$	$Nu_{x2}Re_x^{-\frac{1}{2}}$
1	0.1	1	1	0.5	0.5	0.01	0.01	-5.372235	-1.499065	2.919734	-0.800464
2								4.257771	-11.287344	2.720275	-0.743383
3								14.081198	-21.266923	2.536967	-0.695401
1	0.2							-7.322601	0.406542	3.547017	-0.955236
	0.3							-9.285216	2.302281	4.256245	-1.100276
	0.1	-1.5						27.000264	-17.126646	1.339051	0.030548
		0						7.717805	-7.673976	2.205878	-0.489554
		1	5					-5.749896	-1.791556	2.907950	-0.794768
			10					-6.201901	-2.139557	2.894148	-0.788068
			1	1				-4.490114	-1.690618	2.878460	-0.780429
				5				-3.092135	-1.304449	2.850515	-0.766739
				0.5	1			-6.201901	-2.139557	6.672012	-4.211954
					1.5			-6.201901	-2.139557	60.222764	-44.112047
					0.5	0.1	0.1	-10.339406	-3.578452	3.142022	0.103743
						0.2	0.2	-20.516253	-6.821710	4.158312	1.446942

Conclusion

This paper examines the effect of magnetic field and heat generation on the squeezing flow of Casson hybrid nanofluid between two parallel plates. The problem is modelled using continuity, momentum, and energy equations, which are transformed into dimensionless ODEs via similarity transformations and solved with MATLAB's bvp4c algorithm. The accuracy of the bvp4c algorithm is validated by comparing skin friction results with existing data, showing notable agreement. Numerical results are graphically visualized to analyze the impact of various physical parameters on velocity profile, temperature profile, skin friction coefficient, and Nusselt number. The significant findings of this study are as follows:

(i) An increase in the squeezing parameter Sq and the heat source/sink parameter Q enhances the fluid velocity while the increase in S and M reduces the fluid velocity.
(ii) An increase in Sq, S, λ, and Q raises the temperature profile, while increasing the values of M and β leads to a decrease in the temperature profile.
(iii) For increasing value of λ, wall shear stress and heat transfer increases at the lower plate but decreases at the upper plate.
(iv) As M and Q increases, the wall shear stress declines at both plates while the heat transfer increases at lower plate and decrease at upper plate.
(v) Casson parameter β are positively correlated with the wall shear stress at both plates.
(vi) As β increases, heat transfer rate drops at the lower plate and rises at the upper plate
(vii) As the magnetic parameter M increases, the fluid velocity experiences deceleration at the lower plate, while exhibiting acceleration near the upper plate.
(viii) The enhancement of magnetic M, and injection parameter S can lead to the development of the lower plate's heat transfer performance.
(ix) When the concentrations of nanoparticles increase, the wall shear stress decreasing while heat transfer rate increasing.

Acknowledgement

The author would like to thank all people who have given support for the completion of this proceeding.

References

[1] Wooldridge, M., & Luebbers, R.H. (2020). Heat transfer. *AccessScience*.
[2] Xuan, Y., & Li, Q. (2000). Heat transfer enhancement of nanofluids. *International Journal of Heat and Fluid Flow*, 21(1), 58-64.
[3] Apmann, K., Fulmer, R., Scherer, B., Good, S., Wohld, J., & Vafaei, S. (2022). Nanofluid Heat Transfer: Enhancement of the Heat Transfer Coefficient inside Microchannels. *Nanomaterials (Basel)*, 12(4), 615.
[4] Shah, T. R., Koten, H., & Ali, H. M. (2020). Performance effecting parameters of hybrid nanofluids. *Hybrid Nanofluids for Convection Heat Transfer* (179-213).
[5] George, H. F., & Qureshi, F. (2013). Newton's law of viscosity, Newtonian and nonNewtonian fluids. *Encyclopedia of Tribology*.
[6] Moatimid, G.M., Mohamed, M.A.A. & Elagamy, K. (2022). A Casson nanofluid flow within the conical gap between rotating surfaces of a cone and a horizontal disc. *Sci Rep* 12, 11275.
[7] Abdelmalek, Z., Hussain, A., Bilal, S., Sherif, E.-S. M., & Thounthong, P. (2020). Brownian motion and thermophoretic diffusion influence on thermophysical aspects of electrically conducting viscoelastic nanofluid flow over a stretched surface. *Journal of Materials Research and Technology*, 9(5), 11948-11957.
[8] Louis, S. P., Ushak, S., Milian, Y., Nemś, M., & Nemś, A. (2022). Application of Nanofluids in Improving the Performance of Double-Pipe Heat Exchangers— 54 A Critical Review. *Materials*, 15(19), 6879.
[9] Kamsuwan, C., Wang, X., Seng, L. P., Xian, C. K., Piemjaiswang, R., Piumsomboon, P., Pratumwal, Y., Otarawanna, S., & Chalermsinsuwan, B. (2023). Simulation of nanofluid micro-

channel heat exchanger using computational fluid dynamics integrated with artificial neural network. *Energy Reports*, 9(Supplement 1), 239-247.

[10] Ali, A., Farooq, H., Abbas, Z., Bukhari, Z., & Fatima, A. (2020). Impact of Lorentz force on the pulsatile flow of a non-Newtonian Casson fluid in a constricted channel using Darcy's law: a numerical study. *Sci Rep* 10, 10629.

[11] Afikuzzaman, M., & Alam, M. M. (2016). MHD Casson Fluid Flow through a Parallel Plate. *Thammasat International Journal of Science and Technology*, 21(1).

[12] Attia, H. A., & Sayed-Ahmed, M. E. (2010). Transient MHD Couette Flow of a Casson Fluid Between Parallel Plates with Heat Transfer. *Italian Journal of Pure and Applied Mathematics*, 27(19−38).

[13] Al-Hanaya, A., Alotaibi, M., Shqair, M., & Hagag, A. E. (2023). MHD effects on Casson fluid flow squeezing between parallel plates. *AIMS Mathematics*, 8(12), 29440-29452.

[14] Azeman, S. N. A., Azmi, A. Z., Abidin, N. H. Z., & Omar, N. A. (2024). Effect of magnetic flow and convective heat transfer enhancement using hybrid nanofluid: A structured review. *Journal of Advanced Research in Fluid Mechanics and Thermal Sciences*, 115(2), 13-32.

[15] Klemeš, J. J., & Varbanov, P. S. (2018). Heat transfer improvement, energy saving, management and pollution reduction. *Energy,* 162, 267-271.

[16] Khashi'ie, N. S., Waini, I., Arifin, N. M., & Pop, I. (2021). Unsteady squeezing flow of Cu-Al2O3/water hybrid nanofluid in a horizontal channel with magnetic field. *Scientific Reports*, 11(14128).

[17] Jyothi, A. M., Kumar, R. S. V., Madhukesh, J. K., Prasannakumara, B. C., & Ramesh, G. K. (2021). Squeezing flow of Casson hybrid nanofluid between parallel plates with a heat source or sink and thermophoretic particle deposition. *Heat Transfer*, 50(7), 7139-7156.

[18] Naduvinamani, N. B., & Shankar, U. (2019). Thermal-diffusion and diffusion-thermo effects on squeezing flow of unsteady magneto-hydrodynamic Casson fluid between two parallel plates with thermal radiation*. Sādhanā*, 44, 175.

[19] Takabi, B., & Salehi, S. (2014). Augmentation of the heat transfer performance of a sinusoidal corrugated enclosure by employing hybrid nanofluid. *Advances in Mechanical Engineering*, 2014.

[20] Oztop, H. F., & Abu-Nada, E. (2008). Numerical study of natural convection in partially heated rectangular enclosures filled with nanofluids. *International 55 Journal of Heat and Fluid Flow*, 29(5), 1326–1336.

[21] Waini, I., Ishak, A., & Pop, I. (2020a). MHD flow and heat transfer of a hybrid nanofluid past a permeable stretching/shrinking wedge. *Applied Mathematics and Mechanics (English Edition),* 41(3), 507–520.

[22] Shahzad, F., Jamshed, W., Nisar, K. S., Nasir, N. A. A. M., Safdar, R., Abdel-Aty, A. H., & Yahia, I. S. (2022). Thermal analysis for Al2O3 –sodium alginate 55 magnetized Jeffrey's nanofluid flow past a stretching sheet embedded in a porous medium. *Scientific Reports*, 12(1), 1–14.

[23] Yaseen, M., Rawat, S. K., Shafiq, A., Kumar, M., & Nonlaopon, K. (2022). Analysis of Heat Transfer of Mono and Hybrid Nanofluid Flow between Two Parallel Plates in a Darcy Porous Medium with Thermal Radiation and Heat Generation/Absorption. *Symmetry*, 14(9).